Am J Cancer Res 2022;12(7):3357-3372
www.ajcr.us /ISSN:2156-6976/ajcr0144275

Original Article

Gentian violet induces apoptosis and ferroptosis via modulating p53 and MDM2 in hepatocellular carcinoma

Jingyi Chen[1*], Fangxin Zhao[1,2*], Hongxin Yang[1], Jianxun Wen[1], Ying Tang[1], Fang Wan[3], Xuan Zhang[1], Jianqiang Wu[1,2]

[1]College of Basic Medicine, Inner Mongolia Medical University, Hohhot, Inner Mongolia, China; [2]School of Life Sciences, Inner Mongolia University, Hohhot, Inner Mongolia, China; [3]School of Life Sciences, Inner Mongolia Agricultural University, Hohhot, Inner Mongolia, China. [*]Equal contributors.

Received May 20, 2022; Accepted June 29, 2022; Epub July 15, 2022; Published July 30, 2022

Abstract: Hepatocellular carcinoma (HCC) is the fifth most common malignancies with limited curative options and poor prognosis. Gentian violet (GV) has recently been found to have anti-tumor properties with promising clinical applications. However, its anti-tumor effect and the underlying functional mechanisms in HCC have not been investigated. In this study, we found that GV induced ferroptosis and apoptosis, inhibited cell proliferation, migration and invasion in a dose-dependent manner *in vitro,* and significantly attenuated the growth of HCC *in vivo*. Both ferroptosis inhibitor Ferrostain-1 (Fer-1) and apoptosis inhibitor Z-VAD-KFM (Z-VAD) partially attenuated GV-induced growth-inhibitory effects, while combined treatment of Fer-1 and Z-VAD completely abolished GV's activities. Increased levels of intracellular reactive oxygen species (ROS) were detected after GV treatment. Interestingly, GV elevated the expression levels of both p53 and its negative regulator MDM2, which was dependent on the expression of the dehydrogenase/reductase protein Hep27. Simultaneously silencing both the MDM2 and p53 genes by siRNAs abolished ROS production and partially rescued the cell death induced by GV treatment. Our data demonstrate a GV-Hep27-MDM2-p53 signaling cascade that regulates ferroptosis and apoptosis. Furthermore, our findings provide insights into understanding the anti-tumor function of GV and present the basis of new therapeutic strategies for the treatment of HCC.

Keywords: Gentian violet, hepatocellular carcinoma, ferroptosis, p53, MDM2

Introduction

Hepatocellular carcinoma (HCC) is one of the most common malignancies, and its prognosis remains unsatisfactory. The average five-year survival rate is only about 20% but can be as low as 2.5% in patients with advanced metastatic HCC [1]. Finding new pharmaceutical agents or treatment strategies targeting new cellular signaling molecules will facilitate the improvement in the prognosis of HCC. Induction of apoptosis is the primary function of many anti-tumor drugs. Ferroptosis, a novel type of regulated cell death (RCD) biochemically distinct from apoptosis, has also been found to play an important role in the anti-tumor mechanisms of some drugs. Accumulating evidence shows that ferroptosis is crucial for the treatment of HCC. Indeed, sorafenib, the first-line drug used to treat HCC is an inducer of ferroptosis [2-7].

Recently, GV is emerging as a promising anticancer agent that is economical, relatively safe, and easily available worldwide [8-12]. The anti-tumor property and the underlying mechanisms of GV have been studied in vitro in some cutaneous and non-cutaneous cancers [13-15]. As an FDA approved OTC drug, GV is especially suitable for the experimental treatment of cutaneous cancers, including melanoma and cutaneous lymphomas. Several cases of the topical application of GV to treat cutaneous cancers have been reported with promising efficacy [12, 16, 17]. Our previous studies have shown that GV inhibits cutaneous T cell lymphoma in vitro and ex vivo through the activation of death receptor and mitochondrial apoptotic pathways [10]. Nevertheless, research on the anti-tumor activity and the functional mechanisms of GV is still limited. Most of the studies are focused on either the topical treatment of cutaneous malignancies or *in vitro* investigation of the molecu-

lar mechanisms. *In vivo* study addressing the systemic application of GV for the treatment of solid tumor such as HCC has not been reported.

In this study, to test our hypothesis that GV inhibits the growth of HCC through the induction of apoptosis and ferroptosis, we investigated the effect of the intraperitoneal injection of GV on the growth of HCC in a xenograft mouse model and explored the molecular mechanisms underlying the tumor-suppressing function of GV in HCC. Our studies validated for the first time the effectiveness of the systemic application of GV for the treatment of non-cutaneous tumor and revealed a novel mechanism through which GV induces ferroptosis as well as apoptosis to achieve its anti-tumor effect.

Materials and methods

Cell lines, reagents, and animals

The human hepatocarcinoma cell lines SK-HEP-1 and SMMC-7721 were obtained from the Zhong Qiao Xin Zhou Biotechnology (Shanghai, China), and were cultured at 37°C/5% CO_2 condition using MEM and RPMI-1640 medium supplemented with 10% FBS, respectively. GV, 2,7-dichlorofluorescein diacetate (DCFDA), Ferrostatin-1 (Fer-1), Z-VAD-FMK (Z-VAD) and Necrostatin-1 were purchased from Sigma-Aldrich (St. Louis, USA). CCK-8 kit was from Dojindo (Shanghai, China). Annexin V-FITC/PI apoptosis detection kits was from Beyotime (Shanghai, China). RNA extraction kit and RT-qPCR kit were from TAKARA (Takara Bio, Japan). Six-week-old female BALB/c nude mice were obtained from SiPeiFu Biotechnology (Beijing, China).

Cell viability and colony formation assays

Cells were treated with different concentrations of GV or vehicle (DMSO). Cell death was determined by flow cytometry using Annexin V/PI staining. Cell viability was measured by CCK-8 assay following the manufacturer's instruction. In some experiments, MTT [3-(4, 5-dimethylthiazol-2-yl)-2,5-diphenyltetrazolium bromide] assay was also used to determine cell viability to validate the results from CCK-8 assay. For colony formation assay, cells were seeded into six-well plates at 3000 cells/well and treated with different concentrations of GV or DMSO (50 and 100 nM GV for SK-HEP-1, 150 and 300 nM for SMMC-7721) for 2 weeks. For Fer-1 rescue assays, cells were pre-treated with 2 μM of Fer-1 for 24 h and then treated with GV or DMSO at the indicated concentrations. Colonies with a minimal diameter of 1.0 mm were counted.

Wound healing assay

Cells were plated in the well of six-well plates, and scratches were made using the pipette tips when cell density reached 70-80% confluency. Cells were then treated with GV (50 or 100 nM GV for SK-HEP-1, 150 or 300 nM for SMMC-7721) or DMSO, respectively. For Fer-1 rescue assays, cells were pre-treated with 2 μM of Fer-1 for 24 h and then treated with GV or DMSO at the indicated concentrations. Cell images in wounded areas were captured 24 h before and after treatment. Cell migration distance was analyzed by Image J software.

Transwell invasion assay

Transwell assay was performed with chambers coated with Matrigel. Briefly, cells (1×10^6) in serum free medium containing different concentration of GV (50 or 100 nM GV for SK-HEP-1, 150 or 300 nM for SMMC-7721), or DMSO were respectively seeded into the upper chamber for 24 h, while the lower chamber was added with a medium containing serum. For Fer-1 rescue assays, cells were pre-treated with 2 μM of Fer-1 for 24 h and then treated with GV or DMSO at the indicated concentrations. The invaded cells were fixed with 4% paraformaldehyde and stained with 0.1% gentian violet solution. The number of invaded cells was counted and calculated by Image J software.

Flow cytometry

Flow cytometry was used to detect the live, dead, and apoptotic cells. Briefly, cells were treated with GV (100 nM or 200 nM for SK-HEP-1, and 300 nM or 600 nM for SMMC7721) or DMSO for 48 h (pre-treated with 2 μM Fer-1 for 24 h for rescue assays), resuspended into single-cell suspension, and stained with Annexin V-FITC and PI for 15 min in dark before measurement. For the detection of intracellular ROS, cells were treated with GV or DMSO as described above, stained with 2,7-dichlorofluorescein diacetate (DCFDA) for 30 min, and assayed by flow cytometry. The flow cytometry data were analyzed using FlowJo software.

Reverse transcription and quantitative polymerase chain reaction (RT-qPCR)

Total RNA was extracted, and mRNA was reverse-transcribed into cDNA. qPCR was performed using the following primers: p53: 5'-GAGGTTGGCTCTGACTGTACC-3' (forward) and 5'-TCCGTCCCAGTAGATTACCAC-3' (reverse), MDM2: 5'-TGCCAAGCTTCTCTGTGAA-3' (forward) and 5'-CGATGATTCCTGCTGATTGA-3' (reverse), β-actin: 5'-ATCACCATTGGCAATGAGCG-3' (forward) and 5'-TTGAAGGTAGTTTCGTGGAT-3' (reverse). The relative gene expression level was calculated using the comparative Ct method and normalized to β-actin.

siRNA transfection

Knockdown of MDM2, p53 and Hep27 was performed using siRNA technology. siRNA oligos targeting MDM2 (sc-29394), p53 (sc-29435), Hep27 (sc-92153) or non-specific siRNAs were purchased from Santa Cruz Biotechnology (Dallas, TX). siRNAs were transfected into cells by electroporation using Nucleofector Device and the Nucleofector Kit L (Lonza, Basel, Switzerland). Briefly, 3×10^6 cells were centrifuged and resuspended in 100 μl of transfection solution L, and siRNA was added to a final concentration of 1 mM. Nucleofector program X-001 was used for transfection. Cells were then cultured for 3 days before used in experiments.

Western blotting

Total protein was extracted using RIPA buffer (Solarbio, Beijing, China), resolved on SDS-PAGE, transferred to PVDF membrane, and probed with primary antibodies: Anti-p53 (Cell Signaling, 1:1000), Anti-MDM2 (Cell Signaling, 1:1000), Anti-Hep27 (Cell Signaling, 1:1000), and Anti-GAPDH (Cell Signaling, 1:1000). The membranes were subsequently probed with HRP-conjugated anti-IgG (Cell Signaling, 1:1000) antibody, and then detected with the enhanced chemiluminescence detection kit (Beyotime, Shanghai, China). The protein bands were visualized using a biomolecular imager.

Xenograft mouse model

All animal experiments were performed following the ARRIVE guidelines and carried out in accordance with the Animals (Scientific Procedures) Act, 1986 and associated guidelines. To establish xenograft tumors, 1×10^6 SK-HEP-1 cells were resuspended in 100 μl of serum-free DMEM medium (Gibco, Shanghai, China), and subcutaneously inoculated in the right flank of BALB/c nude mice (n=5/group). Six days after injection, mice bearing xenograft HCC tumor were treated with saline only, or with different dosages of GV (1 mg/kg or 5 mg/kg) in the form of 20% GV solution by intraperitoneal injection every 6 days. Tumor growth was monitored every 3 days for 21 days. Tumor size was measured using calipers. Tumor volume was calculated by the following formula: volume = (longest diameter × shortest diameter^2)/2. The mice were euthanized 3 weeks after treatment, and the tumor samples were dissected for further analysis.

Statistical analysis

The software GraphPad Prime 8.0 and Image J were used for the statistical analysis of data and image processing. Student's t test was used to compare data between two groups. All experiments were repeated three times independently. Data were presented as mean ± SD. $P<0.05$ was considered statistically significant.

Results

GV induced cell death and inhibited cell proliferation

To characterize the general inhibitory effect of GV on HCC cells, we first determined the IC_{50} value of GV by treating two HCC cell lines, SK-HEP-1 and SMMC-7721, with different concentrations of GV for 48 h, and cell viability assay was performed. As shown in **Figure 1A**, GV treatment at concentrations from 0.32 nM to 1000 nM (5 fold dilution, 6 points) for SK-HEP-1 and 8 nM to 25000 nM (5 fold dilution,6 points) for SK-HEP-1 led to a dose-dependent cell growth inhibition in both cell lines. The IC_{50} values were 90 nM for SK-HEP-1 and 338 nM for SMMC-7721 cells. We also examined the changes of proliferation after treating the cells with 50 and 100 nM GV for SK-HEP-1, and 150 and 300 nM for SMMC-7721 up to 3 days. Compared with DMSO treated cells, cells treated with GV showed significantly decreased cell proliferation at both concentrations (**Figure 1B**). Next, to observe the maximum killing

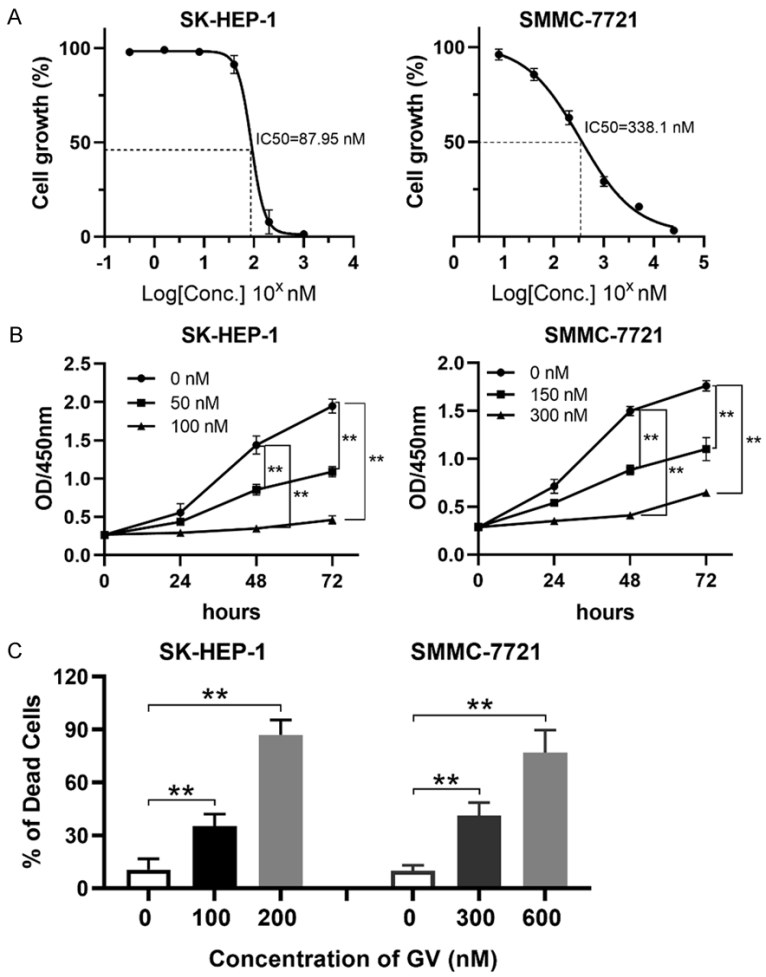

Figure 1. GV induced cell death and inhibited cell proliferation in HCC. A. IC50s of GV in the two cell lines. SK-HEP-1 and SMMC-7721 cells were treated at the indicated concentrations for 48 h. Cell viability was detected by CCK8 assay, and IC50s were calculated. B. The cell growth curves. SK-HEP-1 and SMMC-7721 cells were treated with the indicated concentrations of GV or DMSO for 3 days, and the cell viability was detected by CCK8 assay. C. The total killing rates in the two cell lines. Cells were treated with 100 or 200 nM (SK-HEP-1), and 300 or 600 nM (SMMC-7721) of GV for 48 h, stained by Annexin V/PI, and examined by flow cytometry, Total dead cells were determined by excluding the non-stained cells. Data were presented as mean ± SD. **p<0.01.

effect of GV on HCC, we measured the total percentage of cell death when cells were treated with GV at concentrations of 100 nM or 200 nM for SK-HEP-1, and 300 nM or 600 nM for SMMC-7721 (≈2×IC_{50}), respectively, for 48 h. Cells were stained by Annexin V/PI and analyzed by FlowJo software, and the total killing rates were calculated by excluding the non-stained (double negative) cells. The killing rates were also confirmed by trypan blue cell staining. As shown in **Figure 1C**, the total cell death rates were 35%, 87% and 41%, 77% at the concentrations described above for SK-HEP-1 and SMMC-7721 cells, respectively.

GV inhibited colony formation, migration, and invasion of HCC cells

To investigate the ability of cell survival, colony formation assay was used for both cell lines. The results showed that the number and size of colony were significantly decreased in GV (50 and 100 nM GV for SK-HEP-1, 150 and 300 nM for SMMC-7721) treated cells in a dose-dependent manner (**Figure 2A**). We also explored the effect of GV on the migration and invasion of HCC cells. Cells were treated with the concentrations described above for 24 h. Wound healing assay and Transwell invasion assay were used to evaluate the abilities of migration and invasion, respectively. As shown in **Figure 2B**, **2C**, compared with DMSO treatment, GV treatment significantly inhibited HCC cell migration and invasion in a dose-dependent manner.

GV induced apoptosis in HCC

To distinguish among the types of cell death induced by GV treatment, we first determined whether GV induced apoptosis in SK-HEP-1 and SMMC-7721 cells. Cells were treated with different concentrations of GV for 48 h and analyzed by flow cytometry. The detection of apoptotic cells by Annexin V/PI staining revealed that GV significantly increased both the early and late apoptotic populations at concentrations of 100-200 nM in SK-HEP-1 (MFI was changed from 7% to 32% and 58%) and 300-600 nM in SMMC-7721 cells (MFI was changed from 6% to 21% and 73%) (**Figure 3**). These results suggested the induction of apoptosis by GV.

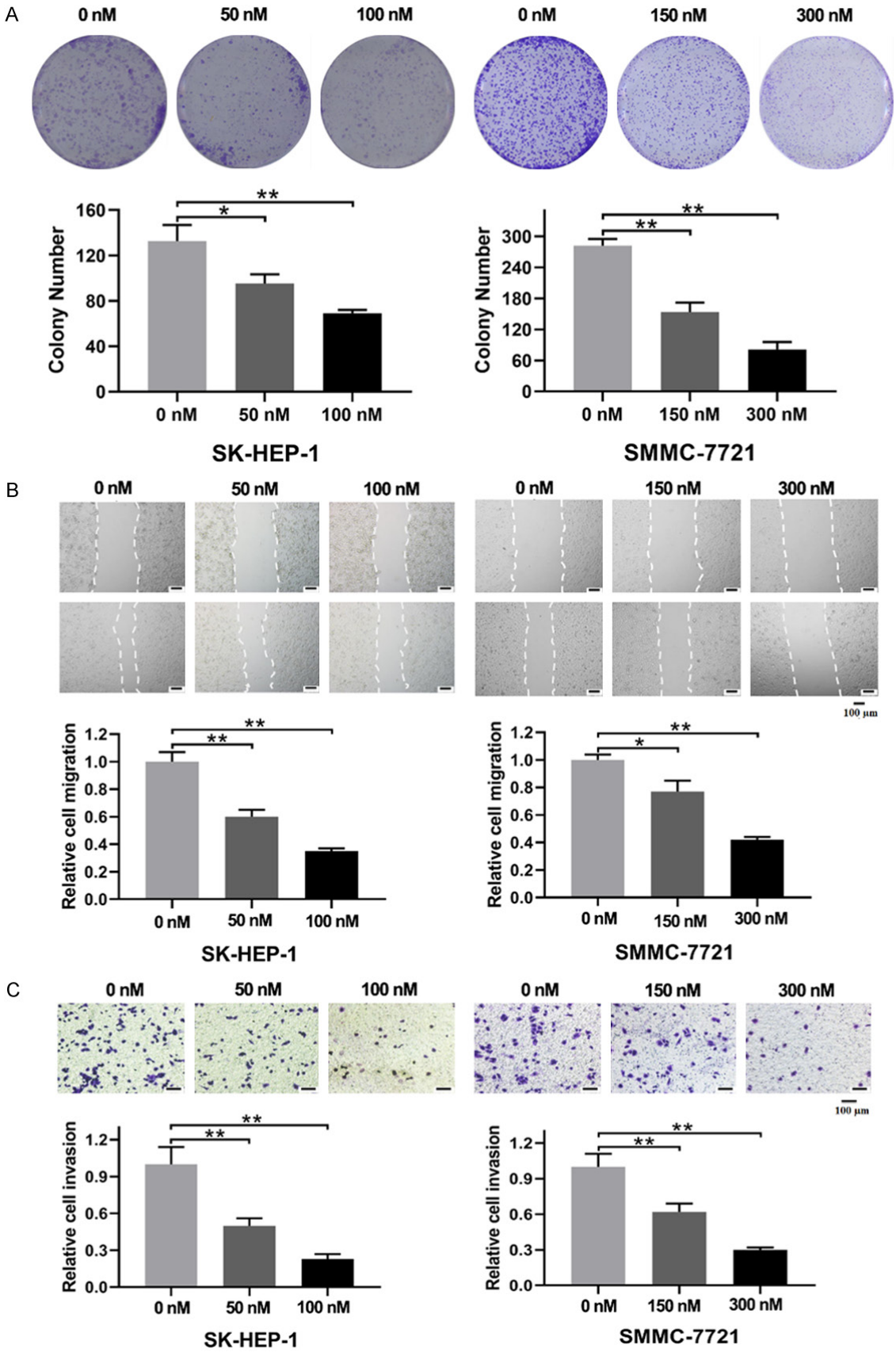
A
0 nM
50 nM
100 nM
0 nM
150 nM
300 nM
Colony Number
SK-HEP-1
SMMC-7721
B
Relative cell migration
100 μm
C
Relative cell invasion

Figure 2. GV inhibited the colony formation, migration, and invasion of HCC cells. A. Representative pictures of the colony formation assay of SK-HEP-1 and SMMC-7721 cells. Histogram demonstrated the statistical analysis of the number of colonies at the indicated GV concentrations. B. Representative pictures of the wound healing assay. Scale bar: 100 μm. Histogram showed the statistical analysis of the migration of the cells treated at the indicated GV concentrations. C. Representative pictures of the Transwell assay. Scale bar: 100 μm. Histogram showed the statistical analysis of the invasion of the cells treated at the indicated GV concentrations. Data were presented as mean ± SD. *P<0.05, **P<0.01.

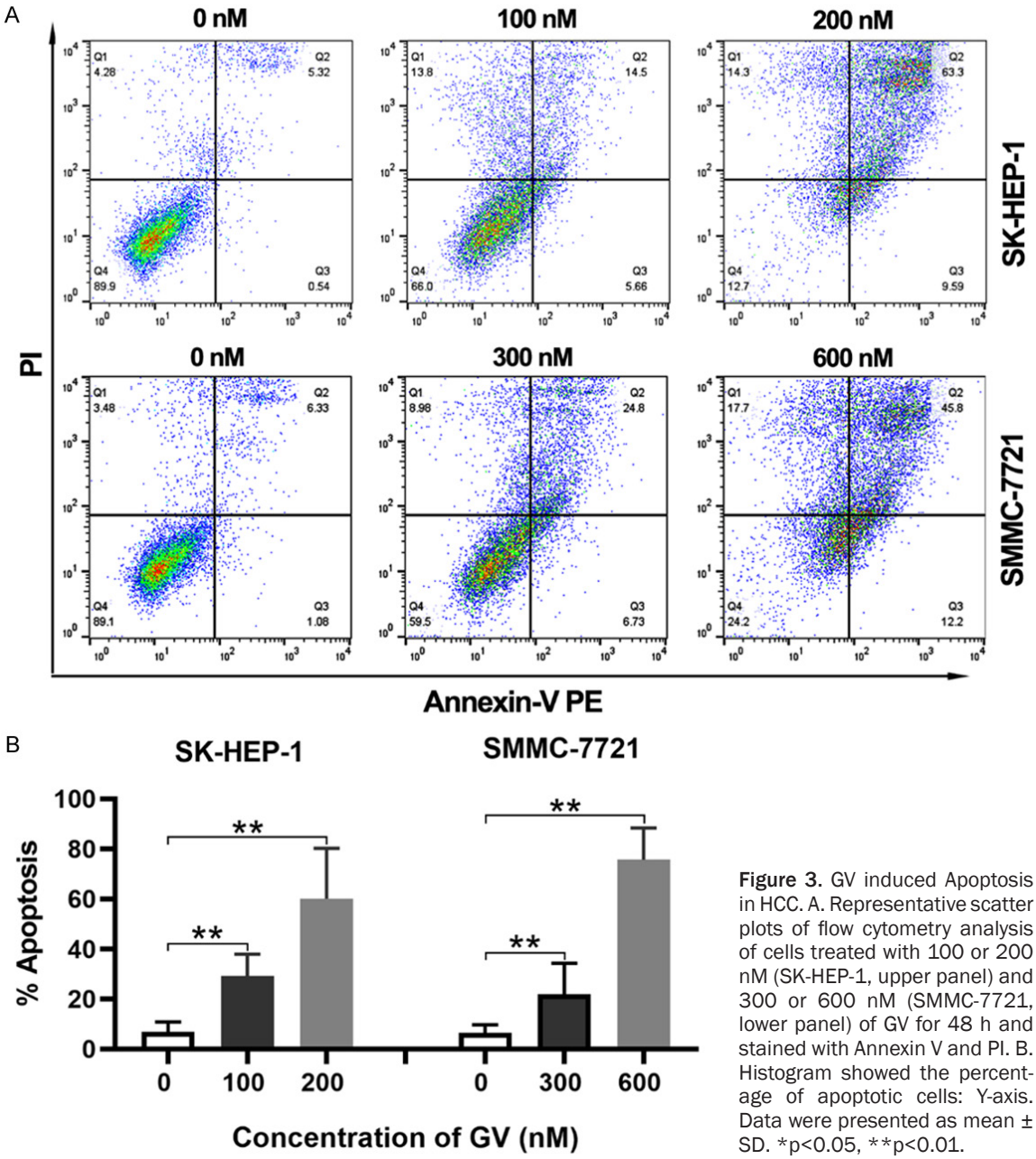

Figure 3. GV induced Apoptosis in HCC. A. Representative scatter plots of flow cytometry analysis of cells treated with 100 or 200 nM (SK-HEP-1, upper panel) and 300 or 600 nM (SMMC-7721, lower panel) of GV for 48 h and stained with Annexin V and PI. B. Histogram showed the percentage of apoptotic cells: Y-axis. Data were presented as mean ± SD. *p<0.05, **p<0.01.

GV induced ferroptosis in HCC

Next, we investigated whether GV induced ferroptosis in SK-HEP-1 and SMMC-7721 cells. In our previous studies on the mechanisms of the tumor-suppressing function of GV in HCC, we have utilized RNA-seq for the transcriptome profiling of GV-treated SK-HEP-1 cells. Pathway enrichment analysis of differentially expressed genes suggested that ferroptosis signaling

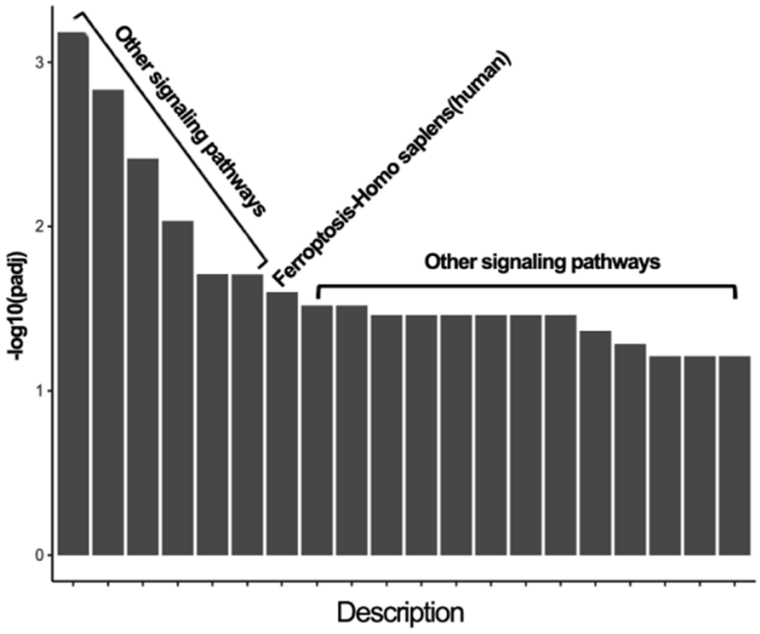

Figure 4. Enriched signaling pathways in GV treated SK-HEP-1 cells. RNA-seq analysis for KEGG pathways significantly enriched with upregulated genes in GV-treated SK-HEP-1 cells. X-axis represents the pathway of DEGs enriched (only Ferroptosis pathway is indicated in the figure). Y-axis represents the Qvalue.

pathway, among other signaling pathways, might be involved in GV-induced cell death (**Figure 4**). To confirm this, in our current study, we used ferroptosis-specific inhibitor Fer-1, apoptosis-specific inhibitor Z-VAD and necrosis inhibitor Necrostain-1 (Nec-1) to differentiate the effect of ferroptosis from the other forms of cell death. SK-HEP-1 and SMMC-7721 cells were treated with GV alone or in combination with Fer-1 (2 μM), Z-VAD (10 μM), Nec-1 (10 μM), or Fer-1 plus Z-VAD, respectively. We found that Fer-1 or Z-VAD significantly attenuated GV-induced cell death with Z-VAD exhibiting a stronger effect than Fer-1. Specifically, the GV-induced cell death was decreased from 82% to 26% in SK-Hep-1 cells and from 89% to 31% in SMMC-7721 cells by Z-VAD treatment. Co-treatment of Fer-1 reduced the cell death from 82% to 60% in SK-Hep-1 cells and from 89% to 64% in SMMC-7721 cells. Strikingly, Combination of Fer-1 and Z-VAD treatment completely abolished the cell death induced by GV, while Nec-1 had no effect (**Figure 5**). Furthermore, colony formation assay, wound healing assay and transwell invasion assay showed that Fer-1 (2 μM) could partially abrogated GV-induced cell proliferation, migration, and invasion in both SK-HEP-1 and SMMC-7721 cells. Taken together, these data indicated that GV-induced inhibition of proliferation, invasion and migration were partially mediated by ferroptosis.

GV induced ROS generation

Increased ROS generation plays a key role in the induction of ferroptosis. Previous studies have indicated that GV causes elevated intracellular ROS levels in lymphoma and melanoma cells [10, 13]. To explore whether GV increases the intracellular ROS level in HCC cells, we measured the production of ROS by flow cytometry. The results showed that ROS levels were significantly elevated after GV treatment. To prove that the accumulation of ROS was partially due to the activation of ferroptosis signaling, we investigated the influences of Fer-1 and Z-VAD on GV-induced ROS generation. Indeed, co-treatment of Fer-1 with GV reduced the generation of ROS, whereas Z-VAD had no on GV-induced ROS generation (**Figure 6**).

GV simultaneously increased MDM2 and p53 expression in vitro and in vivo

Given that p53 plays a key role in the activation of ferroptosis, we explored the effect of GV on the expression of p53. Since the expression of p53 is modulated by its negative regulator MDM2, we also examined the expression level of MDM2 upon GV treatment in SK-HEP-1 and SMMC-7721 cells. As shown in **Figure 7**, GV treatment led to an elevated expression of p53, and, surprisingly, an increased level of MDM2 as well, at both mRNA and protein levels, as determined by RT-qPCR and Western Blot. Immunohistochemical staining of our xenograft tumor samples also showed an increased p53 and MDM2 expression by GV treatment *in vivo*.

GV-induced upregulation of MDM2 and p53 was Hep27-dependent

From the data above, we found that GV treatment increased both MDM2 and p53 levels,

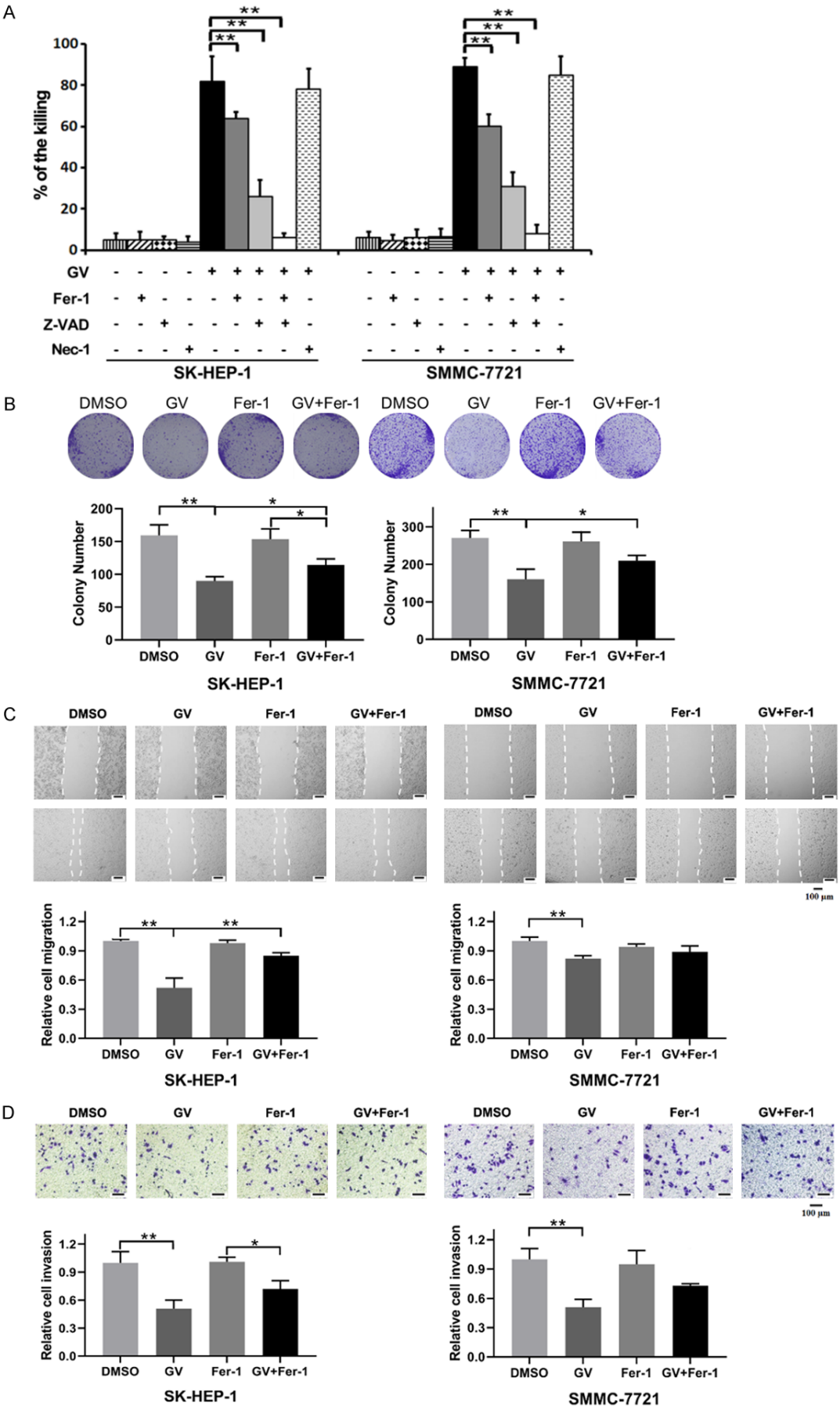
A
% of the killing
GV
Fer-1
Z-VAD
Nec-1
SK-HEP-1
SMMC-7721
B
DMSO
GV
Fer-1
GV+Fer-1
Colony Number
SK-HEP-1
SMMC-7721
C
Relative cell migration
SK-HEP-1
SMMC-7721
100 μm
D
Relative cell invasion
SK-HEP-1
SMMC-7721
100 μm

Figure 5. GV induced ferroptosis in HCC. (A) Analysis of cell death in HCC cells after GV and combined GV, Fer-1 and (or) Z-VAD treatments for 48 h, compared with that in control-treated cells. (B) Representative pictures and histogram figures of analysis of colony formation assay after GV, Fer-1, and GV+Fer-1 treatments for 2 weeks, compared with that in DMSO-treated cells. Wound-healing (C) and transwell invasion (D) assays after GV, Fer-1, and GV+Fer-1 treatments for 24 h, compared with that in DMSO-treated cells. **p<0.01.

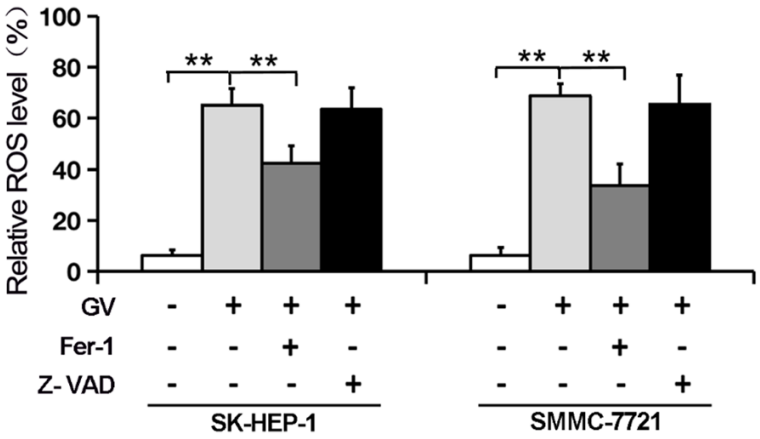

Figure 6. GV induced ROS generation. Cells were treated with DMSO, GV (100 and 300 nM for SK-HEP-1 and SMMC-7721 cells respectively), GV+fer-1 (2 μM) and GV+Z-VAD (10 μM) for 24 h. ROS levels was determined by flow cytometry using 2,7-dichlorofluorescein diacetate (DCFDA) staining. Y-axis showed the relative ROS level. The white, light gray, dark gray and black columns represented DMSO, GV, GV+fer-1 and GV+Z-VAD treatment, respectively. **p<0.01.

suggesting that MDM2 lost its inhibitory effect on p53 level under GV treatment. Since Hep27 is a MDM2 binding protein that stabilizes p53 [18], we speculated that Hep27 might be involved in regulating the stability of p53 and MDM2. To test this, we first examined the influence of GV on the expression of Hep27 in HCC. We found that GV treatment increased the expression level of Hep27 (**Figure 7**). Next, we investigated if MDM2 level was modulated by Hep27. We used Hep27-specific siRNA to silence Hep27 gene expression. Hep27 silencing abolished the high expression levels of MDM2 and p53 induced by GV at both transcript and protein levels, as determined by qRT-PCR and Western Blot. In addition, we also examined the effect of Fer-1 on GV-induced high expression of MDM2 and p53. Compared with GV only treatment, Fer-1 co-treatment did not affect the expression of MDM2 and p53 (**Figure 8**).

GV-induced ferroptosis was dependent on MDM2 and p53

Furthermore, we investigated whether GV-induced ROS production and ferroptosis were dependent on MDM2 and p53. We used MDM2- and p53-specific siRNA to knockdown the expression of MDM2 and p53 to generate MDM2 (-) cells and p53 (-) cells and treated these cells with GV (100 nM for SK-HEP-1 and 300 nM for SMMC-7721) for 3 days after siRNA transfection. Cell viability assay showed that MDM2 silencing alone attenuated GV-induced cell death to the similar level as the effect of Fer-1 (2 μM) treatment in MDM2 (+) cells. However, treatment of MDM2 (-) cells with Fer-1 did not further reduce GV-induced cell death (**Figure 9**). Similarly, the GV activity was also impaired by p53 silencing. However, Fer-1 treatment in p53 (-) cells could further rescue GV-induced cell death. Consistent with the cell viability assay, ROS production was decreased when MDM2 or p53 was silenced by siRNAs (date not shown).

GV inhibited HCC tumor growth in xenograft mouse model

More importantly, to examine the effect of GV on HCC tumor growth *in vivo*, we established xenograft HCC tumor model in BALB/c nude mice. Mice bearing HCC cell-derived tumors were treated with saline, 1 mg/kg, or 5 mg/kg of GV by intraperitoneal injection. Tumor volumes were measured for 3 weeks. As shown in **Figure 10**, GV treatment significantly suppressed the tumor growth in a dose-dependent manner. GV treatment had no effect on the body weight of mice, suggesting that the systemic delivery of GV through intraperitoneal injection was well tolerated by mice.

Discussion

Current research in GV's tumor-suppressing function is mainly focused on *in vitro* study and

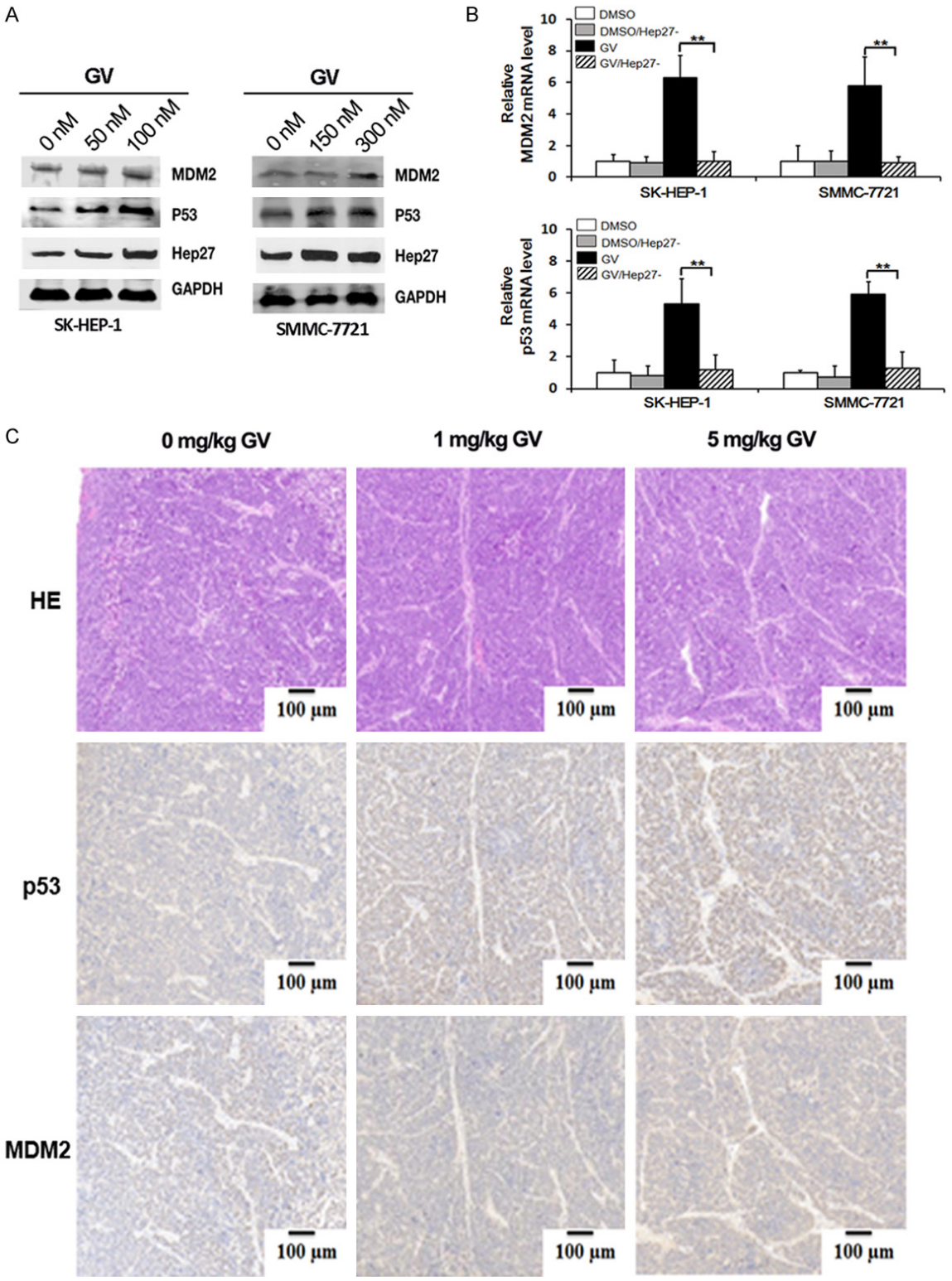

Figure 7. GV simultaneously increased the expression levels of MDM2 and p53. A. SK-HEP-1 and SMMC-7721 cells were treated without or with GV at the concentration of 50, 100 nM or 150, 300 nM respectively, for 48 h. Immunoblot was carried out with the indicated antibodies. B. qRT-qPCR results showing the relative fold changes of MDM2 and p53 mRNA expression at the same treatment condition. C. Representative images of the H&E staining, and the p53 and MDM2 immunohistochemical (IHC) staining of the xenograft tumor tissues. Data were presented as mean ± SD. **p<0.01.

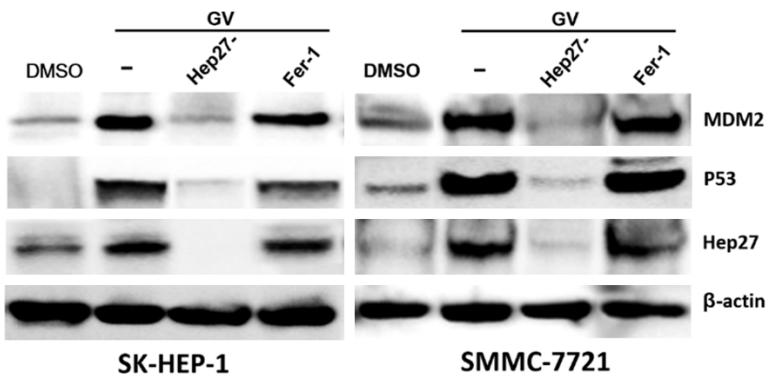

Figure 8. The high expression of MDM2 and p53 was dependent on Hep27. Western blot detection of MDM2, p53 and Hep27 expression in SK-HEP-1 and SMMC-7721 cells at the indicated treatment conditions for 48 h. From left to right for each cell line: DMSO, GV (100 nM for SK-HEP-1 and 300 nM for SMMC-7721), GV in cells transfected with Hep27 siRNA, GV co-treated with Fer-1 (2 μM).

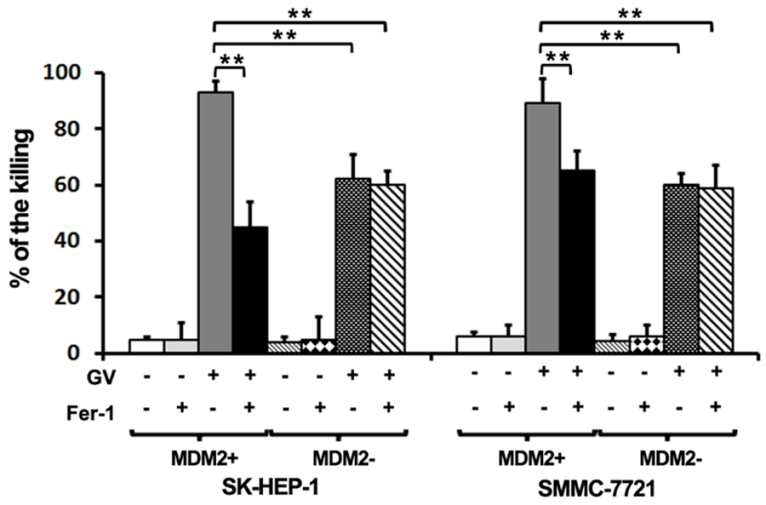

Figure 9. The influences of MDM2 knockdown on GV-induced killing of HCC. Cells were transfected with MDM2-targeting siRNAs or non-specific siRNAs and continue to culture for 24 h. MDM2 (+) and MDM2 (-) cells were treated with DMSO, GV (100 nM for SK-HEP-1 and 300 nM for SMMC-7721), Fer-1 (2 μM), and GV+Fer-1, respectively, for 48 h. Cells were stained with Annxin V/PI and detected by flow cytometry. Total dead cells were determined by excluding the non-stained cells. Y-axis showed the percentage of cell death. **P<0.01.

the topical application of GV for clinical treatment of cutaneous malignancies. However, *in vivo* research on GV's effectiveness in treating other types of cancers, i.e., those without skin manifestations, will be more significant for the broad clinical application of GV. For this purpose, we chose one of the most common solid tumors, HCC, as the model of our study. For the route of GV administration, we used intraperitoneal (IP) injection. With IP, pharmaceutical molecules can be completely absorbed into systemic circulation similar to intravenous (IV) administration [19]. We demonstrated in this study that GV induced HCC cell death and suppressed tumor growth *in vivo*. By using IP injection of GV in xenograft HCC mouse model, we validated for the first time the effectiveness of the systemic application of GV for the treatment of non-cutaneous solid tumor. In addition, we found GV given through systemic administration was well tolerated. Hence, our findings provide the experimental basis for the potential treatment of HCC by GV, and more, the potential application of GV in the treatment of a wide range of tumors via systemic administration.

Most anti-tumor drugs induce cancer cell death through different types of cell death such as apoptosis, ferroptosis and necrosis. Among them, apoptosis is the most common type of programmed cell death triggered by anti-tumor drugs. Previous studies have found that GV induces apoptosis through death receptor and mitochondrial apoptotic pathways in cutaneous T-cell lymphoma and other types of cancer cells [10, 15, 20-22]. In our current study, we confirmed the GV-induced apoptosis in HCC, as determined by Annexin V/PI staining and rescue experiments with apoptosis inhibitor V-ZAD.

In our previous studies in investigating how GV influenced the transcriptome of HCC cells, we performed an RNA-seq analysis in SK-HEP-1 cells treated with or without GV. Enriched pathway analysis of the RNA-seq data suggested that ferroptosis signaling might be involved in GV-induced cell death. Ferroptosis, a type of

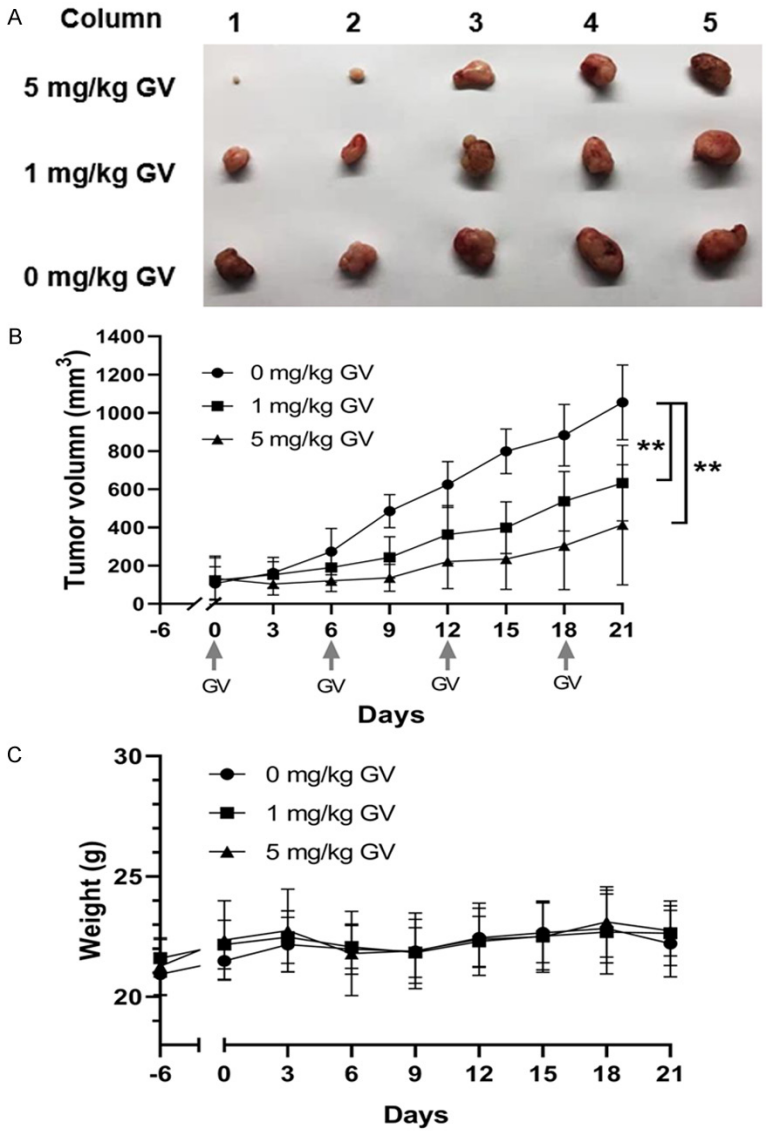

Figure 10. GV inhibited HCC tumor growth in xenograft mouse tumor model. A. The image of representing tumors surgically dissected from 5 groups of mice (columns 1-5) treated with 0, 1 mg, and 5 mg (GV)/kg (body weight) of GV, respectively, at the end of observation (21st day). B. Tumor growth curves as measured and calculated every 3 days for 21 days. C. The body weight changes of mice for each group during the 21-day treatment. Data were presented as mean ± SD. **P<0.01.

regulated cell death (RCD), is mediated by iron-dependent lipid peroxidation. It can be induced by its specific inducer erastin and several anti-tumor drugs and blocked by its specific inhibitor Fer-1. Fer-1 blocks lipid hydroperoxide generation, which is the key step in the initiation of ferroptosis. The ability of Fer-1 to attenuate GV-induced cell death indicated the involvement of ferroptosis [6, 22, 23]. Although induction of ferroptosis has been regarded as a new promising strategy for the treatment of cancers, including HCC [6, 24, 25], whether GV can activate ferroptosis signaling in cancer cells has never been investigated. In this study, we found for the first time that GV triggers ferroptosis, in addition to apoptosis, in HCC. Therefore, GV executes its anti-tumor function through the activation of both apoptosis and ferroptosis, but not necrosis, as indicated by the assays using specific necrosis inhibitor Nec-1. Apoptosis contributed more than ferroptosis in GV-induced cell death, as shown by the percentages of apoptotic and ferroptotic cells detected. These results extended our understanding on the activity and functional mechanisms of GV and provided the rationale for the combinational therapy using GV with other drugs to achieve synergistic effects in cancer treatment.

The increase of ROS production is a key step in both mitochondrial apoptosis and ferroptosis [6]. We have shown previously that GV increases ROS to enhance the transcription of FAS ligand, thereby triggering FAS pathway-induced apoptosis in T cell lymphoma [10]. It has also been reported that GV can inhibit NADPH oxidase (NOX), the main source of cellular ROS generation, which may lead to a decreased ROS production in certain biological contexts [15]. However, in other circumstances, GV fails to decrease ROS level, and on the contrary, increases ROS production in cancer cells [13]. The mechanisms underlying GV's contradicted effect on ROS generation are not clear, although it is known that depending on cell type or treatment, ROS may be involved in either tumor-promoting or tumor-suppressing signal-

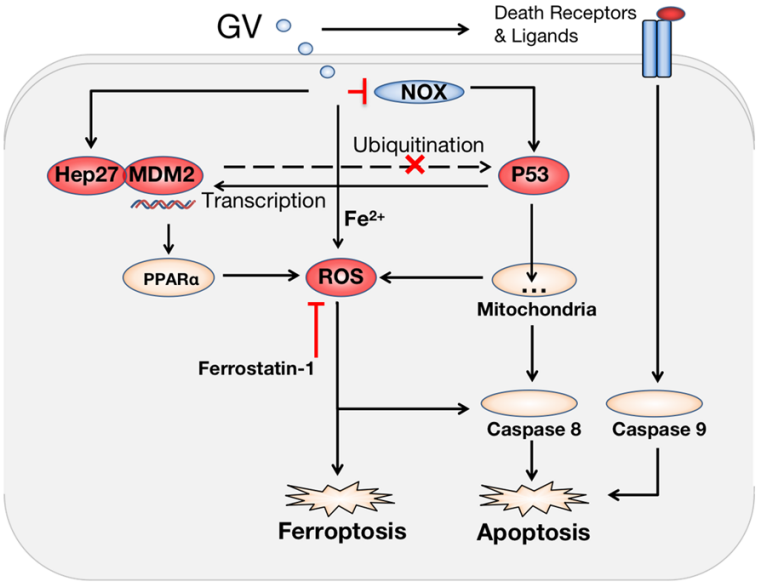

Figure 11. The proposed molecular mechanisms of GV-induced killing of HCC. When NOX is inhibited by GV, Hep27 is increased, which leads to the blockade of the ubiquitination and degradation of p53 by MDM2. Consequently, the levels of p53 and MDM2 are increased. GV also directly increases p53 level. Increased p53 and MDM2 levels trigger ferroptosis and mitochondrial apoptosis (through the activation of caspase 8) by a coordinated ROS cross point and downstream signaling cascades. On the other hand, GV also triggers death receptor apoptosis (through the activation of caspase 9) by upregulating death receptors DR4/5 and ligands FAS-ligand and TRAIL.

ing in cancer cells [26]. In this study, we found that GV led to elevated ROS that could be partially blocked by Fer-1, suggesting that ferroptosis signaling regulated ROS generation. Hence, as diagramed in **Figure 11**, we propose that ROS may act as a central mediator connecting and regulating both apoptosis and ferroptosis in GV-induced cell death. Because Fer-1 blocks ferroptosis but does not influence caspase-3-dependent apoptosis, in which ROS also plays an important role [27], we also examined the influence of pan-caspase inhibitor V-ZAD on ROS generation. The results showed that V-ZAD did not affect ROS generation, which could be explained that caspases are downstream of ROS in the apoptotic pathway.

In addition to its role in promoting apoptosis, the well-known tumor suppressor p53 has recently been found to induce ferroptosis [9, 28-31]. Several lines of evidence have indicated that GV upregulates p53 in melanoma, lung cancer, colon cancer and glioblastoma cell lines [13, 21, 32]. Here, our results showed that p53 was significantly upregulated by GV treatment in HCC. The signaling pathways mediating the GV effect on p53 are not clear; however, one possible mechanism is via NOXs. GV has been shown to suppress NOXs [15]. Since NOX-1 inhibits p53 expression, GV may induce p53 expression by abrogating NOX1-mediated P53 inhibition.

The p53-binding protein MDM2 is an E3 ubiquitin ligase that suppresses p53 level. In normal condition, p53 induces the transcription of MDM2, which, in turn, constitutively suppresses p53 by ubiquitinating and targeting p53 for degradation to form a negative feedback loop, maintaining the basal expression levels of both p53 and MDM2 [33]. Unexpectedly, we found that MDM2 level was also elevated simultaneously with p53 by GV treatment, suggesting MDM2 and p53 may function coordinately during GV-induced cell death different from their normal crosstalk. In supporting this, published studies have found that MDM2 may function as a context-dependent tumor suppressor despite its established role as an oncoprotein inhibiting p53 [10]. importantly, MDM2 has been found to facilitate ferroptosis independent of p53 by lipid remodeling through forming a complex with MDMX and altering PPAR activity [34]. Given that p53 and MDM2 are simultaneously up-regulated, we proposed that MDM2 functions as a tumor suppressor in GV-mediated cellular responses. It loses p53-ubiquiting ability and indirectly augments apoptosis through the accumulation of p53. High expression of MDM2 may also act directly to promote ferroptosis by activating PPAR activity.

The increased levels of MDM2 and p53 by GV treatment suggested that GV regulated the activity of the negative feedback circuit of the p53-MDM2 pair. To understand the molecular mechanism of this regulation, we investigated the role of MDM2 binding protein Hep27 (Dehydrogenase/reductase SDR family member 2, DHRS2), downregulation of which was

significantly associated with the worse outcome of cancer patients [35]. Hep27 is a mitochondrial protein and a NADPH-dependent oxidoreductase that can translocate to nucleus and inhibit MDM2 by binding to it and consequently stabilizing p53. Hep27 expression is positively correlated with the levels of MDM2 and p53 [18]. With increased Hep27 binding, MDM2 loses its inhibiting feedback effect on p53. Accumulation of p53 leads to an enhanced p53-induced transcription of MDM2. Hep27-MDM2 binding may also prevent MDM2 from degradation. In our study, knockdown of Hep27 by siRNA abolished GV-induced high expression of MDM2 and p53. However, Fer-1 treatment did not influence the high expression of MDM2 and p53 caused by GV (**Figure 8**). This could be explained that Fer-1 blocked the lipid peroxidation and affected ROS production downstream of ferroptosis signaling [7]; however, it did not inhibit the upstream components, such as MDM2 and p53, in ferroptosis signaling (**Figure 11**).

Increased levels of MDM2 and p53 contribute to GV-mediated cancer cell death by different but cooperative signaling pathways. For example, MDM2 and p53 both activate ferroptosis signaling but p53 also promotes apoptosis through caspase-dependent signaling [10, 31]. Notably, Hep27 is a reductase and diminishes ROS by nature. Since GV increases cellular ROS, we hypothesized that the coexistence of high levels of Hep27 and ROS might be critical for the function of GV-induced cell death.

In our study, we found that MDM2 knockdown by siRNA attenuated the GV-induced cell death. This MDM2 effect was not influenced by the additional treatment of Fer-1 but was similar to the inhibitory effect of Fer-1 in GV-treated MDM2 (+) cells, suggesting that the induction of ferroptosis by GV was dependent on the elevated MDM2. On the other hand, p53 knockdown by siRNA also reversed the GV-induced cell death; However, additional Fer-1 treatment could further reverse the GV-induced cell death. These results, together with the data from Hep27 silencing experiments, indicated that elevated MDM2 played a key role in the induction of ferroptosis, which was mainly through the GV-Hep27-MDM2-p53 axis in HCC. The proposed mechanism of GV-induced HCC cell death was diagrammed in **Figure 11**.

Current treatment options for HCC are still limited. GV has several advantages, such as its availability worldwide, low price, and well tolerance when used topically, which makes it a good candidate for a broad utilization. Here, we provide evidence from *in vitro* and *in vivo* studies that GV induces apoptosis and ferroptosis leading to tumor inhibition in HCC. GV-induced ferroptosis is through the generation of ROS and the high expression of p53 and MDM2. Hence, we reveal a novel mechanism of GV's function, which is dependent on an Hep27-MDM2-p53 signaling cascade. Our findings suggest that GV is a potential effective agent for the treatment of HCC and provide the rational for a further investigation in applying GV for the treatment of other types of cancer.

Acknowledgements

This work was supported by the Inner Mongolia Science & Technology Project Plan (2019-GG037). Inner Mongolia Medical University Science and Technology Project (YKD2018-KJBW027).

Disclosure of conflict of interest

None.

Address correspondence to: Drs. Jianqiang Wu and Xuan Zhang, College of Basic Medicine, Inner Mongolia Medical University, Hohhot 010000, Inner Mongolia, China. E-mail: jianqiangwu@immu.edu.cn (JQW); zhxuan024@163.com (XZ)

References

[1] Zhou Y, Wang L, Ban X, Zeng T, Zhu Y, Li M, Guan XY and Li Y. DHRS2 inhibits cell growth and motility in esophageal squamous cell carcinoma. Oncogene 2018; 37: 1086-1094.

[2] Liao H, Shi J, Wen K, Lin J, Liu Q, Shi B, Yan Y and Xiao Z. Molecular targets of ferroptosis in hepatocellular carcinoma. J Hepatocell Carcinoma 2021; 8: 985-996.

[3] Chen S, Zhu JY, Zang X and Zhai YZ. The emerging role of ferroptosis in liver diseases. Front Cell Dev Biol 2021; 9: 801365.

[4] Nie J, Lin B, Zhou M, Wu L and Zheng T. Role of ferroptosis in hepatocellular carcinoma. J Cancer Res Clin Oncol 2018; 144: 2329-2337.

[5] Lachaier E, Louandre C, Godin C, Saidak Z, Baert M, Diouf M, Chauffert B and Galmiche A. Sorafenib induces ferroptosis in human cancer cell lines originating from different solid tumors. Anticancer Res 2014; 34: 6417-6422.

[6] Wang HT, Ju J, Wang SC, Zhang YH, Liu CY, Wang T, Yu X, Wang F, Cheng XR, Wang K and Chen ZY. Insights into ferroptosis, a novel target for the therapy of cancer. Front Oncol 2022; 12: 812534.
[7] Miotto G, Rossetto M, Di Paolo ML, Orian L, Venerando R, Roveri A, Vučković AM, Bosello Travain V, Zaccarin M, Zennaro L, Maiorino M, Toppo S, Ursini F and Cozza G. Insight into the mechanism of ferroptosis inhibition by ferrostatin-1. Redox Biol 2020; 28: 101328.
[8] Maley AM and Arbiser JL. Gentian violet: a 19th century drug re-emerges in the 21st century. Exp Dermatol 2013; 22: 775-780.
[9] Ou Y, Wang SJ, Li D, Chu B and Gu W. Activation of SAT1 engages polyamine metabolism with p53-mediated ferroptotic responses. Proc Natl Acad Sci U S A 2016; 113: E6806-E6812.
[10] Wu J and Wood GS. Analysis of the effect of gentian violet on apoptosis and proliferation in cutaneous T-cell lymphoma in an in vitro study. JAMA Dermatol 2018; 154: 1191-1198.
[11] Arbiser JL. Gentian violet is safe. J Am Acad Dermatol 2009; 61: 359-359.
[12] Arbiser JL, Bips M, Seidler A, Bonner MY and Kovach C. Combination therapy of imiquimod and gentian violet for cutaneous melanoma metastases. J Am Acad Dermatol 2012; 67: E81-E83.
[13] Pietrobono S, Morandi A, Gagliardi S, Gerlini G, Borgognoni L, Chiarugi P, Arbiser JL and Stecca B. Down-regulation of SOX2 underlies the inhibitory effects of the triphenylmethane gentian violet on melanoma cell self-renewal and survival. J Invest Dermatol 2016; 136: 2059-2069.
[14] Yamaguchi M, Vikulina T and Weitzmann MN. Gentian violet inhibits MDA-MB-231 human breast cancer cell proliferation, and reverses the stimulation of osteoclastogenesis and suppression of osteoblast activity induced by cancer cells. Oncol Rep 2015; 34: 2156-2162.
[15] Perry BN, Govindarajan B, Bhandarkar SS, Knaus UG, Valo M, Sturk C, Carrillo CO, Sohn A, Cerimele F, Dumont D, Losken A, Williams J, Brown LF, Tan XL, Ioffe E, Yancopoulos GD and Arbiser JL. Pharmacologic blockade of angiopoietin-2 is efficacious against model hemangiomas in mice. J Invest Dermatol 2006; 126: 2316-2322.
[16] Westergaard SA, Lechowicz MJ, Harrington M, Elsey J, Arbiser JL and Khan MK. Induction of remission in a patient with end-stage cutaneous T-cell lymphoma by concurrent use of radiation therapy, gentian violet, and mogamulizumab. JAAD Case Rep 2020; 6: 761-765.
[17] Rao S, Morris R, Rice ZP and Arbiser JL. Regression of diffuse B-cell lymphoma of the leg with intralesional gentian violet. Exp Dermatol 2018; 27: 93-95.
[18] Deisenroth C, Thorner AR, Enomoto T, Perou CM and Zhang YP. Mitochondrial HEP27 is a c-Myb target gene that inhibits Mdm2 and stabilizes p53. Mol Cell Biol 2010; 30: 3981-3993.
[19] Al Shoyaib A, Archie SR and Karamyan VT. Intraperitoneal route of drug administration: should it be used in experimental animal studies? Pharm Res 2019; 37: 12.
[20] Yamaguchi M and Murata T. Potential suppressive effects of gentian violet on human breast cancer MDA-MB-231 cells in vitro: comparison with gemcitabine. Oncol Lett 2016; 12: 1605-1609.
[21] Garufi A, D'Orazi V, Arbiser JL and D'Orazi G. Gentian violet induces wtp53 transactivation in cancer cells. Int J Oncol 2014; 44: 1084-1090.
[22] Arbiser JL. Gentian violet: bench-to-bedside research that lowers healthcare costs. Skinmed 2016; 14: 91-92.
[23] Zhao S, Zheng W, Yu C, Xu G, Zhang X, Pan C, Feng Y, Yang K, Zhou J and Ma Y. The role of ferroptosis in the treatment and drug resistance of hepatocellular carcinoma. Front Cell Dev Biol 2022; 10: 845232.
[24] Chen Y, Li L, Lan J, Cui Y, Rao X, Zhao J, Xing T, Ju G, Song G, Lou J and Liang J. CRISPR screens uncover protective effect of PSTK as a regulator of chemotherapy-induced ferroptosis in hepatocellular carcinoma. Mol Cancer 2022; 21: 11.
[25] Yu J and Wang JQ. Research mechanisms of and pharmaceutical treatments for ferroptosis in liver diseases. Biochimie 2021; 180: 149-157.
[26] Mukawera E, Chartier S, Williams V, Pagano PJ, Lapointe R and Grandvaux N. Redox-modulating agents target NOX2-dependent IKKepsilon oncogenic kinase expression and proliferation in human breast cancer cell lines. Redox Biol 2015; 6: 9-18.
[27] Zilka O, Shah R, Li B, Friedmann Angeli JP, Griesser M, Conrad M and Pratt DA. On the Mechanism of cytoprotection by ferrostatin-1 and liproxstatin-1 and the role of lipid peroxidation in ferroptotic cell death. ACS Cent Sci 2017; 3: 232-243.
[28] Liu Y and Gu W. p53 in ferroptosis regulation: the new weapon for the old guardian. Cell Death Differ 2022; 29: 895-910.
[29] Liu J, Zhang C, Wang J, Hu W and Feng Z. The regulation of ferroptosis by tumor suppressor p53 and its pathway. Int J Mol Sci 2020; 21: 8387.
[30] Jiang L, Kon N, Li TY, Wang SJ, Su T, Hibshoosh H, Baer R and Gu W. Ferroptosis as a p53-me-

diated activity during tumour suppression. Nature 2015; 520: 57-62.
[31] Kuganesan N, Dlamini S, Tillekeratne LMV and Taylor WR. Tumor suppressor p53 promotes ferroptosis in oxidative stress conditions independent of modulation of ferroptosis by p21, CDKs, RB, and E2F. J Biol Chem 2021; 297: 101365.
[32] Yamaguchi M, Vikulina T, Arbiser JL and Weitzmann MN. Suppression of NF-kappaB activation by gentian violet promotes osteoblastogenesis and suppresses osteoclastogenesis. Curr Mol Med 2014; 14: 783-792.
[33] Meng X, Franklin DA, Dong J and Zhang Y. MDM2-p53 pathway in hepatocellular carcinoma. Cancer Res 2014; 74: 7161-7167.
[34] Venkatesh D, O'Brien NA, Zandkarimi F, Tong DR, Stokes ME, Dunn DE, Kengmana ES, Aron AT, Klein AM, Csuka JM, Moon SH, Conrad M, Chang CJ, Lo DC, D'Alessandro A, Prives C and Stockwell BR. MDM2 and MDMX promote ferroptosis by PPARalpha-mediated lipid remodeling. Genes Dev 2020; 34: 526-543.
[35] Chidambaranathan-Reghupaty S, Fisher PB and Sarkar D. Hepatocellular carcinoma (HCC): epidemiology, etiology and molecular classification. Adv Cancer Res 2021; 149: 1-61.